Optimized Schwarz methods for advection diffusion equations in bounded domains

Martin J. Gander[1] and Tommaso Vanzan[1]

Section de mathématiques, Université de Genève, 2-4 rue du Lièvre, Genève,
{martin.gander},{tommaso.vanzan}@unige.ch

Abstract. Optimized Schwarz methods use better transmission conditions than the classical Dirichlet conditions that were used by Schwarz. These transmission conditions are optimized for the physical problem that needs to be solved to lead to fast convergence. The optimization is typically performed in the geometrically simplified setting of two unbounded subdomains using Fourier transforms. Recent studies for both homogeneous and heterogeneous domain decomposition methods indicate that the geometry of the physical domain has actually an influence on this optimization process. We study here this influence for an advection diffusion equation in a bounded domain using separation of variables. We provide theoretical results for the min-max problems characterizing the optimized transmission conditions. Our numerical experiments show significant improvements of the new transmission conditions which take the geometry into account, especially for strong tangential advection.

1 Introduction

We study optimized Schwarz methods for the advection diffusion equation

$$\begin{aligned} -\nu\Delta u + \mathbf{a}\cdot\nabla u = 0 \quad &\text{in} \quad \Omega, \\ u = g \quad &\text{on} \quad \partial\Omega, \end{aligned} \tag{1}$$

where $\nu \in \mathbb{R}^+$, $\mathbf{a} = (a_1, a_2)^T \in \mathbb{R}^2$ and Ω is a bounded domain in two dimensions. As a model problem we consider the geometry given in Figure 1. We decompose $\Omega = (-L, L) \times (0, L)$ into two subdomains $\Omega_1 = (-L, 0) \times$

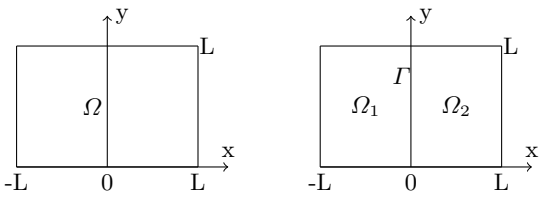

Fig. 1. Geometry of the domain Ω on the left, and decomposition into two subdomains on the right.

$(0,L)$ and $\Omega_2 = (0,L)\times(0,L)$, and because of the linearity of (1), we study the optimized Schwarz methods for the errors $e_j^n = u_j - u_j^n$,

$$\begin{aligned} -\nu\Delta e_1^n + \mathbf{a}\cdot\nabla e_1^n = 0 \ \text{ in } \Omega_1, \quad (\nu\partial_x + s_1)(e_1^n)(0,\cdot) = (\nu\partial_x + s_1)(e_2^{n-1})(0,\cdot),\\ -\nu\Delta e_2^n + \mathbf{a}\cdot\nabla e_2^n = 0 \ \text{ in } \Omega_2, \quad (\nu\partial_x - s_2)(e_2^n)(0,\cdot) = (\nu\partial_x - s_2)(e_1^{n-1})(0,\cdot), \end{aligned} \tag{2}$$

where $s_1, s_2 \in \mathbb{R}$ are to be determined to get fast convergence. This is typically done using Fourier transforms in the simplified setting of unbounded domains, see [1] and references therein, and in particular [2] for the case of advection diffusion problems. Advection diffusion problems have however often boundary layers, which can not be taken into account using unbounded domain analysis. The influence of geometry on the optimization for Laplace's equation on a rectangular domain has been studied in [3], and for circular domain decomposition, see [4],[5]. We study here for the first time the influence of geometry on the optimization of transmission conditions for advection diffusion problems, looking for a separation of variables solution of the form $e_j^n(x,y) = \phi_j^n(x)\psi_j^n(y), j = 1,2$ in rectangular domains. Substituting the separation of variables Ansatz into (1), we obtain on Ω_1

$$\nu\partial_{yy}\psi_1^n - a_2\partial_y\psi_1^n + \lambda\psi_1^n = 0, \quad y \in (0,L), \tag{3}$$
$$\psi_1^n(0) = \psi_1^n(L) = 0,$$
$$\nu\partial_{xx}\phi_1^n - a_1\partial_x\phi_1^n - \lambda\phi_1^n = 0, \quad x \in (-L,0), \tag{4}$$
$$\phi_1^n(-L) = 0 \quad \text{and} \quad \nu\partial_x\phi_1^n(0) + s_1\phi_1^n(0) = r_2^{n-1},$$

where r_2^{n-1} is the Robin data to impose on Γ. Equation (3) is a Sturm-Liouville eigenvalue problem,

$$\mathcal{L}\psi = \lambda\psi,\ \psi(0) = \psi(L) = 0,\ \mathcal{L}\psi := \nu e^{\frac{a_2 y}{\nu}}\left(-\frac{d}{dy}\left[e^{-\frac{a_2 y}{\nu}}\frac{d\psi(y)}{dy}\right]\right). \tag{5}$$

Hence the λ are the eigenvalues of the differential operator $\mathcal{L}$ with the associated boundary conditions, and the eigenfunctions ψ form an orthogonal basis for the Hilbert space $L^2(0,L)$ with respect to the weighted L^2 inner product

$$\langle f,g\rangle_w = \int_0^L f(y)g(y)e^{-\frac{a_2 y}{\nu}}dy, \quad \|f\|_w^2 = \int_0^L f^2 e^{-\frac{a_2 y}{\nu}}dy.$$

For $\lambda \le 0$, equation (5) does not admit a solution due to the boundary conditions. For $\lambda > 0$, the general solution of (5) is given by

$$\psi(y) = e^{\frac{a_2 y}{2\nu}}\left(C_1^n\cos(\sqrt{\frac{4\lambda\nu - a_2^2}{2\nu}}y) + C_2^n\sin(\sqrt{\frac{4\lambda\nu - a_2^2}{2\nu}}y)\right).$$

The boundary conditions prescribe $C_1^n = 0$ and a quantization on λ such that $\lambda = \lambda_l = \frac{\nu\pi^2 l^2}{L^2} + \frac{a_2^2}{4\nu}$, $l \in \mathbb{N}$. Equation (4) then has the associated solution

$$\phi_1^n(x) = e^{\frac{a_1 x}{2\nu}}\left(D_1^n e^{\frac{\sqrt{a_1^2+4\nu\lambda_l}\,x}{2\nu}} + D_2^n e^{-\frac{\sqrt{a_1^2+4\nu\lambda_l}\,x}{2\nu}}\right).$$

Since boundary layers appearing on lateral boundaries will not reach the interface, we assume for simplicity that the domain is unbounded in the x direction and therefore get $D_2^n = 0$. With similar calculations for $e_2(x,y)$, we obtain for the error functions on both subdomains by linearity

$$\begin{aligned} e_1^n(x,y) &= \sum_{l=1}^{\infty} \hat{e}_{1,l}^n e^{\frac{a_1 x + a_2 y}{2\nu}} \sin(\tfrac{l\pi y}{L}) e^{\frac{\sqrt{a_1^2 + a_2^2 + \frac{4\nu^2 l^2 \pi^2}{L^2}}}{2\nu} x}, \\ e_2^n(x,y) &= \sum_{l=1}^{\infty} \hat{e}_{2,l}^n e^{\frac{a_1 x + a_2 y}{2\nu}} \sin(\tfrac{l\pi y}{L}) e^{-\frac{\sqrt{a_1^2 + a_2^2 + \frac{4\nu^2 l^2 \pi^2}{L^2}}}{2\nu} x}, \end{aligned} \tag{6}$$

where $\hat{e}_{j,l}^n$ are constants to be determined imposing the Robin transmission conditions on Γ. Inserting the series expansions for e_1^n,e_2^n into the transmission conditions of the optimized Schwarz methods (2) and using the orthonormality of the eigenfunctions, we find for each l

$$\begin{aligned} \left(\tfrac{a_1}{2} + \tfrac{\sqrt{a_1^2 + a_2^2 + \frac{4\nu^2 l^2 \pi^2}{L^2}}}{2} + s_1 \right) \hat{e}_{1,l}^n &= \left(\tfrac{a_1}{2} - \tfrac{\sqrt{a_1^2 + a_2^2 + \frac{4\nu^2 l^2 \pi^2}{L^2}}}{2} + s_1 \right) \hat{e}_{2,l}^{n-1}, \\ \left(\tfrac{a_1}{2} - \tfrac{\sqrt{a_1^2 + a_2^2 + \frac{4\nu^2 l^2 \pi^2}{L^2}}}{2} - s_2 \right) \hat{e}_{2,l}^n &= \left(\tfrac{a_1}{2} + \tfrac{\sqrt{a_1^2 + a_2^2 + \frac{4\nu^2 l^2 \pi^2}{L^2}}}{2} - s_2 \right) \hat{e}_{1,l}^{n-1}. \end{aligned} \tag{7}$$

We thus obtain over a double step $\hat{e}_{1,l}^n = \rho(l)\hat{e}_{1,l}^{n-2}$, $\hat{e}_{2,l}^n = \rho(l)\hat{e}_{2,l}^{n-2}$, where the convergence factor is given by

$$\rho(l) := \frac{\sqrt{a_1^2 + a_2^2 + \frac{4\nu^2 l^2 \pi^2}{L^2}} - a_1 - 2s_1}{\sqrt{a_1^2 + a_2^2 + \frac{4\nu^2 l^2 \pi^2}{L^2}} - a_1 + 2s_2} \frac{\sqrt{a_1^2 + a_2^2 + \frac{4\nu^2 l^2 \pi^2}{L^2}} + a_1 - 2s_2}{\sqrt{a_1^2 + a_2^2 + \frac{4\nu^2 l^2 \pi^2}{L^2}} + a_1 + 2s_1}. \tag{8}$$

2 Optimization

To optimize s_1, s_2 for fast convergence, we need to minimize the absolute value of the convergence factor $\rho(l)$ over all relevant $l \in \{1, \ldots, N\}$, where N is determined by the numerical truncation of the infinite series[1]. We introduce the function $f : p \to \sqrt{a_1^2 + a_2^2 + 4\frac{\nu^2 p^2 \pi^2}{L^2}}$, and set first $s_1 := \frac{f(p) - a_1}{2}$ and $s_2 := \frac{f(p) + a_1}{2}$, where $p \in \mathbb{R}^+$, since f depends on p^2. Inserting these expressions for s_1, s_2 into (8), and considering for simplicity a continuous set for l instead of the discrete one, see [9], we obtain the min-max problem

$$\min_{p \in \mathbb{R}^+} \max_{l \in [1,N]} |\rho(l,p)| = \min_{p \in \mathbb{R}^+} \max_{l \in [1,N]} \left| \left(\frac{f(l) - f(p)}{f(l) + f(p)} \right)^2 \right|. \tag{9}$$

[1] In the unbounded domain analysis, one minimizes over all frequencies $k := \frac{\pi l}{L} \in [k_{\min}, k_{\max}]$, with $k_{\min} := \frac{\pi}{L}$ and $k_{\max} = \frac{\pi}{h}$, where $h = \frac{L}{N+1}$ is the mesh size and N the number of mesh points on the interface Γ. From (6), we see that $k_{\min}$ corresponds to $l = 1$, and for $l = N$, $\frac{\pi N}{L} \approx \frac{\pi}{h} = k_{\max}$, like in e.g. [1].

We now solve the general min-max problem (9) under the only condition that the function f is strictly monotonic, which holds for our case.

Theorem 1. *If the function f is strictly monotonic, then the solution of the min-max problem* (9) *is given by the unique p^* which satisfies $f(p^*) = \sqrt{f(1)f(N)}$.*

Proof. We prove the result when f is strictly increasing, the argument when f is strictly decreasing is analogous. Since the objective function is squared, we can omit the absolute value, and we compute

$$\frac{\partial \rho}{\partial l} = \frac{4(f(l)-f(p))f_l(l)f(p)}{(f(l)+f(p))^3}, \quad \frac{\partial \rho}{\partial p} = -\frac{4(f(l)-f(p))f_p(p)f(p)}{(f(l)+f(p))^3}, \tag{10}$$

where f_l, f_p are the derivatives of f with respect to l and p. If $p < l$ for every l then, since f is strictly increasing, we know that $f(l) > f(p)$ and $f_p(p) > 0$, therefore $\frac{\partial \rho}{\partial p} < 0$ and we can not be at the optimum since increasing p decreases $\max_{l\in[1,N]} |\rho(l,p)|$. The same argument holds if $p > N$ and we conclude that at the optimum $p \in [1,N]$. Due to the monotonicity of f, the convergence factor has a unique zero at $l = p$, and from the partial derivative with respect to l, we see that $\rho(l,p)$ has only two local maxima located at $l = 1$ and $l = N, \forall p \in [1,N]$. Therefore, $\max_{l\in[1,N]} |\rho(l,p)| = \max\{\rho(1,p), \rho(N,p)\}$. Now since $\frac{\partial \rho(1,p)}{\partial p} > 0 \ \forall p \in (1,N]$ and $\frac{\partial \rho(N,p)}{\partial p} < 0 \ \forall p \in [1,N)$, by continuity the optimal p^* satisfies $\rho(1,p) = \rho(N,p)$. The uniqueness of p^* follows from the strict sign of $\frac{\partial \rho(l,p)}{\partial p}$ for $l = 1, N$ and a direct computation leads to $f(p^*) = \sqrt{f(1)f(N)}$.

Theorem 2. *When $N \to +\infty$, the asymptotic behaviour of the optimized Schwarz method given by Theorem 1 is*

$$\max_{1\le l\le N} |\rho(l,p^*)| = 1 - \frac{2\sqrt{2}\ \sqrt[1/4]{(a_1^2+a_2^2)L^2+4\nu^2\pi^2}}{\sqrt{\nu\pi}} \frac{1}{\sqrt{N}}, \tag{11}$$

where $p^* = \sqrt{\sqrt{a_1^2 + a_2^2 + \frac{4\nu^2\pi^2}{L^2}}\frac{L}{2\pi\nu}}\sqrt{N}$.

Proof. We make the Ansatz $p^* = C_p N^\alpha$ and we solve the equation $f(p^*) = \sqrt{f(1)f(N)}$ asymptotically.

We consider now the more general case where s_1, s_2 depend on two different parameters, $s_1 = \frac{f(p)-a_1}{2}$ and $s_2 = \frac{f(q)+a_1}{2}$, with $p, q \in \mathbb{R}^+$, and study

$$\min_{p,q\in\mathbb{R}^+} \max_{l\in[1,N]} |\rho(l,p,q)| = \min_{p,q\in\mathbb{R}^+} \max_{l\in[1,N]} \left| \left(\frac{f(l)-f(p)}{f(l)+f(p)}\right)\left(\frac{f(l)-f(q)}{f(l)+f(q)}\right)\right|. \tag{12}$$

Theorem 3. *If the function f is strictly monotonic, then the solution of the min-max problem* (12) *is given by two couples (p_j^*, q_j^*), $j = 1, 2$ which satisfy $|\rho(1, p, q)| = |\rho(\hat{l}, p, q)| = |\rho(N, p, q)|$, where $\hat{l}$ is an interior local maximum such that $f(\hat{l}) = \sqrt{f(p)f(q)}$, and we have $p_2^* = q_1^*$ and $q_2^* = p_1^*$.*

Proof. We observe that $\rho(l, p, q)$ is invariant if we exchange p and q, therefore we focus our attention on the case $p < q$. The sign of the partial derivatives with respect to p and q satisfies

$$\operatorname{sign}\left(\frac{\partial|\rho|}{\partial p}\right) = \operatorname{sign}\left(-f(l) + f(p)\right), \quad \operatorname{sign}\left(\frac{\partial|\rho|}{\partial q}\right) = \operatorname{sign}\left(-f(l) + f(q)\right).$$

Repeating the argument of Theorem 1, we obtain that at the optimum we must have $p, q \in [1, N]$. For the derivative with respect to l, we obtain

$$\frac{\partial|\rho|}{\partial l} = \operatorname{sign}(\rho(l, p, q)) \frac{2f_l(l)(f(p) + f(q))(f(l)^2 - f(q)f(p))}{(f(l) + f(p))^2(f(l) + f(q))^2}.$$

We thus have three local maxima with respect to l, one located at $l = 1$, one at $l = N$, and an interior local maximum at $\hat{l}$, with $p < \hat{l} < q$ which is the unique zero of the partial derivative, satisfying $f(\hat{l})^2 - f(q)f(p) = 0$. The uniqueness of $\hat{l}$ follows from the strict monotonicity of f. We thus have $\max_{l\in[1,N]} |\rho(l, p, q)| = \max\{|\rho(1, p, q)|, |\rho(\hat{l}, p, q)|, |\rho(N, p, q)|\}$. Now we observe that for $1 < p < q < N$, we have

$$\begin{array}{lll} \partial_p|\rho(1,p,q)| > 0 & \partial_p|\rho(\hat{l},p,q)| < 0 & \partial_p|\rho(N,p,q)| < 0, \\ \partial_q|\rho(1,p,q)| > 0 & \partial_q|\rho(\hat{l},p,q)| > 0 & \partial_q|\rho(N,p,q)| < 0. \end{array} \tag{13}$$

Suppose that $|\rho(1, p, q)| < |\rho(N, p, q)|$. Then from (13), we see that increasing p uniformly improves $\max\{|\rho(1)|, |\rho(\hat{l})|, |\rho(N)|\}$. In the case $|\rho(1, p, q)| > |\rho(N, p, q)|$, similarly decreasing q uniformly improves $\max\{|\rho(1)|, |\rho(\hat{l})|, |\rho(N)|\}$. Thus, at the optimized parameters p^* and q^*, we must have $|\rho(1, p^*, q^*)| = |\rho(N, p^*, q^*)|$, and a direct computation leads to the condition $f(p^*)f(q^*) = f(1)f(N)$. We can thus focus on one parameter only, say p, letting $q = q(p)$, varying such that the constraint $f(p)f(q(p)) = f(1)f(N)$ is satisfied. Since f is strictly increasing, $q(p)$ must be a decreasing function of p in order to satisfy the constraint. Moreover $q(1) = N$ and $q(N) = 1$. We thus obtain the equivalent min-max problem

$$\min_{1\le p\le \hat{l}} \max\{|\rho(1, p, q(p))|, |\rho(\hat{l}, p, q(p))|\}. \tag{14}$$

Combining (13), the implicit differentiation $\frac{dq(p)}{dp} = -\frac{f'(p)f(q(p))}{f'(q(p))f(p)}$ and the explicit expressions for the partial derivatives, we obtain

$$\begin{array}{l} |\rho(1,1,q(1))| = 0,\ |\rho(1,\hat{l},q(\hat{l}))| > 0,\ \frac{d|\rho(1,p)|}{dp} = \frac{\partial|\rho(1,p,q(p))|}{\partial p} + \frac{\partial|\rho(1,p,q(p))|}{\partial q}\frac{dq(p)}{dp} > 0, \\ |\rho(\hat{l},1,q(1))| > 0,\ |\rho(\hat{l},\hat{l},q(\hat{l}))| = 0,\ \ \frac{d|\rho(\hat{l},p)|}{dp} = \frac{\partial|\rho(\hat{l},p,q(p))|}{\partial p} + \frac{\partial|\rho(\hat{l},p,q(p))|}{\partial q}\frac{dq(p)}{dp} < 0. \end{array} \tag{15}$$

These observations are sufficient to conclude, as in the last steps in Theorem 1, that there exists a unique p^*, solution of the min-max problem (14), so that the solution of (12) is given by p^*, solution of (14), and q^* defined implicitly by $f(p^*)f(q^*) = f(1)f(N)$. The same argument can be repeated for the case $1 < q < p < N$, and since $|\rho(l, p, q)|$ is invariant under the change $p \leftrightarrow q$, we obtain the desired result.

3 Numerical Experiments

The transmission conditions for the advection diffusion equation (1) were analyzed in [2] using Fourier transforms assuming unbounded domains in the y direction, which led to the convergence factor

$$\tilde{\rho}(k, s_1, s_2) := \frac{\sqrt{a_1^2-4i\nu a_2 k+4\nu^2k^2}-a_1-2\tilde{s}_1}{\sqrt{a_1^2-4i\nu a_2 k+4\nu^2k^2}-a_1+2\tilde{s}_2} \frac{\sqrt{a_1^2-4i\nu a_2 k+4\nu^2k^2}+a_1-2\tilde{s}_2}{\sqrt{a_1^2-4i\nu a_2 k+4\nu^2k^2}+a_1+2\tilde{s}_1}. \tag{16}$$

This convergence factor was then optimized for $\tilde{s}_1 := \frac{a_1-\tilde{p}}{2\nu}$ and $\tilde{s}_2 := \frac{a+\tilde{p}}{2\nu}$, where we use the tilde to distinguish from our variables s_j and p. Equations (16) and (8) are similar in many aspects, but they differ profoundly in the dependence on the tangential advection a_2 since equation (16) is a complex quantity if $a_2 \neq 0$. This comes directly from the Fourier transform, as the calculations in [2] show, and makes the corresponding min-max problems much harder to solve than the ones proposed here. In addition, our numerical tests below show that our new optimized parameters perform substantially better when strong advection is present along the interface. We discretize the problem using finite differences, and use as initial guess random functions with values in the interval $[-1, 1]$ multiplied by the factor $e^{\frac{a_2 y}{2\nu}}$, so that we introduce errors in all eigenfunction components in (6). Without the weight, a projection on the orthogonal basis (6) showed that the lowest and highest frequencies are statistically less present compared to the intermediate ones, and this leads initially to an artificially faster contraction. We stop the algorithm when both $\|e_1^n|_\Gamma\|_w$ and $\|e_2^n|_\Gamma\|_w$ are less than $\epsilon = 10^{-8}$. This norm corresponds to our analysis, since by Parseval, $\|e_j^n|_\Gamma\|_w = \sum_l |\hat{e}_{j,l}^n|_\Gamma|^2$. For comparison, we will also measure the error in the L^2 norm, which corresponds to using the sine basis, $e_j^n|_\Gamma = \sum_l \bar{e}_{j,l}^n \sin(j\pi y)$, since by Parseval $\|e_j^n|_\Gamma\|_2 = \sum_l |\bar{e}_{j,l}^n|_\Gamma|^2$. We show in Figure 2 two iteration plots: in the left panel, for weak tangential advection, the estimates for the optimal parameters $f(p^*)$ and $\tilde{p}$ are similar; in the right panel, for strong tangential advection, the analysis presented in this manuscript is able to provide a parameter which leads to a more efficient algorithm than $\tilde{p}$. We verified also that the discrepancy between the iteration counts obtained with the two norms disappears when we decrease the tolerance ϵ. In Figure 3, we show the corresponding iteration plots for the two parameter case. For the unbounded domain convergence factor (16), there is no theorem available giving the optimal choice for the parameters, since the complex nature of $|\tilde{\rho}|$ makes the min-max problem extremely difficult to solve, and we thus solved it numerically here.

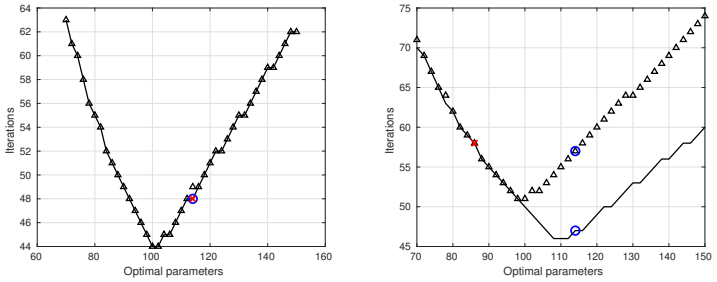

Fig. 2. Iteration numbers for weak tangential advection, $\nu = 1$, $a_1 = 20$, $a_2 = 1$, (left), and strong tangential advection, $\nu = 1$, $a_1 = 1$, $a_2 = 20$ (right). The blue circle corresponds to $f(p^*)$ from the new bounded analysis, and the red cross to $\tilde{p}$ from the unbounded analysis. The continuous black line is for the weighted norm $\|\cdot\|_w$, and the triangle for the standard norm $\|\cdot\|_2$.

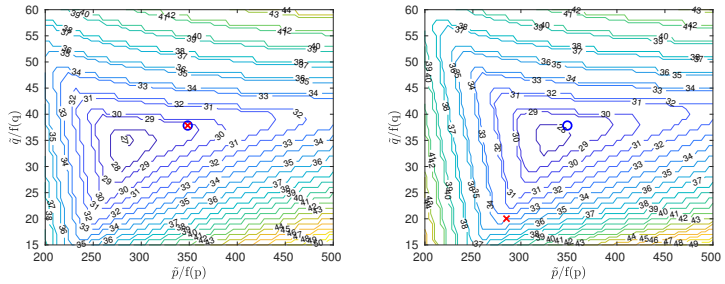

Fig. 3. Iteration numbers for weak tangential advection, $\nu = 1$, $a_1 = 20$, $a_2 = 1$ (left), and strong tangential advection, $\nu = 1$, $a_1 = 1$, $a_2 = 20$ (right). The blue circle stands for the parameters from the new bounded analysis, and the red cross for the ones from the unbounded analysis.

4 Conclusion

The key step in the derivation of the convergence factor is that we could use separation of variables: this allowed us to expand the errors e_j^n in a series of orthogonal eigenfunctions along the interface, and to obtain recursive relations for each frequency, i.e. we could diagonalize the iteration operator, see also [8]. Fourier invented the Fourier transform in his famous treatise on the 'Théorie analytique de la chaleur' from 1822 precisely by using separation of variables, and the success of the Fourier transform is based on the fact that it permits such a diagonalization for many classical PDEs such as diffusion, reaction-diffusion, Helmholtz and, by the way, also an advection-diffusion equation with only normal advection, in the presence of Dirichlet boundary conditions. On unbounded domains, even more differential operators can be diagonalized, also the advection diffusion operator with general

advection term. The presence of the Dirichlet boundary conditions and tangential advection however changes the eigenbasis, see (6), and also the inner product in which the eigenfunctions are orthogonal, it is not $L^2(0,L)$ any more, but a weighted inner product. Since the sine functions are not eigenfunctions of the general advection diffusion operator on the bounded domain, if we started the optimized Schwarz methods with $e_j^0 = \bar{e}_{j,1}^0 \sin(\pi y)$, already after the first iteration, the errors e_j^1 would not be proportional to the same sine function, $e_j^1 \neq \bar{e}_{j,1}^1 \sin(\pi y)$, but contain in general a combination of sine functions, $e_j^1 = \sum_{l=-\infty}^{\infty} \bar{e}_{j,l}^1 \sin(l\pi y)$, and therefore it would not be possible to obtain recursive relations like in (7).

This insight sheds light on the emerging field of heterogeneous optimized Schwarz methods. Great care is needed in the procedure used to obtain the convergence factor. While no issues seem to be present for problems where a common eigenbasis is shared by the PDEs of interest, see [6], recent failures of the standard analysis for more complicated couplings [7] may be traced back to the lack of a shared eigenbasis which leads to an inappropriate derivation of $\rho(l)$.

References

1. M. J. Gander, *Optimized Schwarz Methods*, SIAM J. num. anal, Vol. 44, No. 2 (2006).
2. O. Dubois, *Optimized Schwarz Methods with Robin Conditions for the Advection-Diffusion Equation*, in Domain Decomposition Methods in Science and Engineering XVI, Lecture Notes in Computational Science and Engineering (2006).
3. M. J. Gander,*On the Influence of Geometry on Optimized Schwarz Methods*, Bol. Soc.Esp. Mat. Apl., Num 52, pp. 71-78 (2011).
4. M. J. Gander, Y. Xu, *Optimized Schwarz Methods for Circular Domain Decompositions with Overlap*, SIAM J. Num. Anal., Vol 52, No. 4 (2014).
5. M. J. Gander, Y. Xu,*Optimized Schwarz Methods with Nonoverlapping Circular Domain Decomposition*, Math. of Comp., Vol. 86, No. 304 (2017)
6. M. J. Gander, T. Vanzan, *Heterogeneous Optimized Schwarz Methods for Coupling Helmholtz and Laplace Equations*, accepted for Domain Decomposition Methods in Science and Engineering XXIV, LNCSE, Springer-Verlag, (2018).
7. M. Discacciati, L.G. Giorda, *Optimized Schwarz methods for the Stokes-Darcy coupling*, IMA J. of Num. Anal. (2017).
8. M. J. Gander, Y. Xu, *Optimized Schwarz methods for model problems with continuously variable coefficients*, SIAM J. Sci. Comp., Vol 38, No. 5, pp. A2964–A2986 (2016).
9. S. Loisel,J. Cote, M.J. Gander, L. Laayouni and A. Qaddouri, *Optimized domain decomposition methods for the spherical Laplacian*, SIAM J. Num. Anal., Vol. 48, No. 5, pp. 524–551 (2010).